Nanoalloy composition-temperature phase diagram for catalyst design: Case study of Ag-Au

Lin-Lin Wang,[1,*] Teck L. Tan,[2] and Duane D. Johnson[1,3,†]
[1]*Ames Laboratory, U.S. Department of Energy, Ames, Iowa 50011, USA*
[2]*Institute of High Performance Computing, Agency for Science, Technology and Research, Singapore 138632, Singapore*
[3]*Department of Materials Science and Engineering, Iowa State University, Ames, Iowa 50011, USA*
(Received 6 June 2012; published 23 July 2012)

By coupling a cluster expansion with density functional theory (DFT) calculations, we determine the configurational thermodynamics (site preferences and occupations) for alloyed nanoparticles (NPs) as functions of composition (c) and temperature (T), exemplified using a 55-atom Ag-Au truncated cuboctahedron NP. The c-T phase diagram for site occupations gives detailed design information for alloyed NP, especially the thermodynamically stable active sites for catalysis and how they change with stoichiometry and processing temperature. Generally, Ag prefers core and Au prefers shell, agreeing with our universal core-shell preference assessed from DFT impurity segregation energies but with interesting multishell configurations having specific active sites.

DOI: 10.1103/PhysRevB.86.035438 PACS number(s): 68.65.−k, 81.30.−t, 64.75.−g

I. INTRODUCTION

Alloyed, bimetallic nanoparticles (NPs) have been intensively studied for their unique properties, often different from bulk alloys or NPs of elemental metals. Ag-Au NPs have been found to offer tunable catalytic[1–5] and plasmonic[6,7] properties by varying size and composition. For example, Ag-Au NPs are highly active for low-temperature CO oxidation,[1–3] aerobic oxidation of *p*-hydroxybenzyl,[4] and others.[5] The improved catalytic properties from pure Au NPs have been attributed to a synergistic effect, where Ag helps to activate O_2.[1–3,8] As many studies on model catalysts of surface alloys have shown, such synergistic effects highly depend on the distribution of atoms on different sites,[9–11] i.e., configurational thermodynamics or chemical ordering. For NPs, the existence of many different types of low-coordinated sites on the facets makes such studies more difficult. Experimental studies using techniques such as extended x-ray absorption fine structures[12,13] or high-resolution transmission electron microscopy[14,15] can tell the overall core-shell preference but not specific site preference or occupation on the facets of NPs. Theoretical studies on configurational thermodynamics of NPs directly using first-principles methods, such as density functional theory[16,17] (DFT) calculations, is possible but also difficult due to the enormous number of possible configurations. Here we use the cluster expansion[18] (CE) method with DFT calculations, an approach that has proved to be very successful for bulk alloys,[19–28] to study the configurational thermodynamics of a 55-atom truncated cuboctahedral (TC) NP with face-centered cubic (fcc) stacking. We study the specific site occupations as functions of both composition (c) and temperature (T).

In experiments, both Ag-core/Au-shell and Au-core/Ag-shell with different degrees of alloying and mixing have been observed,[29–36] depending on the synthesis methods and the procedure for which metal ions are reduced first. Exposure to air, solution, or passivating agents can further affect segregation in the Ag-Au NPs. A recent study showed Ag_xO forming on the Ag-Au NPs surface in the absence of ligands or surfactants when exposed to air.[36] In theory, studies using semi-empirical potentials all show Ag segregated to shell because Ag has a smaller surface energy than Au and their atomic sizes are similar.[37–41] But this notion has been challenged by more accurate DFT calculations for small Ag-Au NPs around 1 nm.[42,43] They showed that Au prefers segregation to shell for 13- and 38-atom NPs in many structural motifs, including cuboctahedron, icosahedron, and other low-symmetry structures due to the charge transfer from Ag to Au and the directional bonding of Au. Because of the strong relativistic effect, the strong *s*-*d* hybridization in Au favors structures with low coordination.[44] A recent study using semi-empirical potentials with charge transfer effect included showed that Au segregating to shell for Ag-Au NP as large as 147-atom, agreeing with results from DFT calculations.[45]

Previously, we have used DFT to study the core-shell preference for bimetallic NPs of all late TMs by calculating the segregation energy of an impurity in the 55-atom TC NP[46] and utilized the same analysis for alloyed surfaces. We found a highly correlated sequence of Au, Ag, Cu, Pd, Pt, Ni, Ir, Rh, Co, Os, Ru, and Fe in which the left (right)-most TM has the highest shell (core) preference for most cases, altered in experiment only by adsorption effects, e.g., oxidation. This trend in core-shell preference can help design thermodynamically stable core-shell NP not limiting to binaries. Among several factors often mentioned to determine the core-shell preference, we found that the truly independent factors are only cohesive energy and atomic radius, a universal behavior confirmed by a generic tight-binding analysis reflecting *d*-band filling and *d*-band width, respectively.

Here we extend the generic behavior to include more alloy-specific behavior. Namely, we use CE coupled with DFT calculations to study configurational thermodynamics of alloyed NP, with specific focus on the Ag-Au system. We will detail site occupation beyond just the core-shell preference. For the bulk alloy of Ag-Au, we have shown[28] (besides the dominated attractive 1-body) that a repulsive nearest-neighbor 2-body effective cluster interaction (ECI) controls alloying; thus, Ag and Au favor mixing and unlike nearest neighbors. On the ground state (GS) hull of bulk Ag-Au, it gives three GSs, Cu_3Au-type (or $L1_2$) structure at 25 and 75% Au and Cu-Au (or $L1_0$) structure at 50% Au. For the NP, we study how the low-coordination sites on NP facets induce segregation and

site preferences. From the generic core-shell preference, based on single impurity segregation energy, the Ag prefers the core and Au the shell; so we address how the core-shell preference can be modified by the chemical ordering effect. Specifically, we show that the interplay between surface segregation and mixing stabilizes a multishell configuration for the Ag-Au NP with unique site occupations. The c-T phase diagram of these site occupations provides direct design information for alloyed NP, especially the thermodynamically stable active sites for catalysis.

II. COMPUTATIONAL DETAILS

As a function of occupational variables on a fixed lattice, the CE permits a description of a specific physical quantity as a series of orthogonal cluster correlation functions constructed from the single-site occupation variable.[18] For example,

$$E(\boldsymbol{\sigma}) = \sum_{\alpha} V_{\alpha} \bar{\Phi}_{\alpha}(\boldsymbol{\sigma}), \tag{1}$$

Where $E(\boldsymbol{\sigma})$ is the formation energy of the system, $\bar{\Phi}_{\alpha}(\sigma) = \langle \sigma_1 \sigma_2 \cdots \sigma_{\alpha} \rangle$ is the cluster correlation function averaged over the occupation variables, σ_i, of sites belonging to the α th cluster, and V_{α} is the corresponding ECI calculated via structural inversion.[47] Here, σ_i equals 0 (1) if site i is occupied by Ag (Au). For bulk system, a DFT-based calculation of an alloy (and hence CE) uses a small unit cell with periodic boundary condition (PBC). Notably, the definition of CE is independent of translational or point group symmetries, which serve to reduce the number of nonequivalent clusters. For the loss of PBC in a NP, it is equivalent to consider a large unit cell with all atoms in the NP treated as the CE basis but restricted to the cell at the origin with the inclusion of enough vacuum to eliminate the undesired interactions among the repeating images of the NP. For example, we use a cubic cell of 20 Å for the 55-atom NP. Similar strategy has been successfully used to construct a layer-wise CE to study segregation for alloy surfaces.[48]

We use an iterative approach to find both the optimal ECI and GS. With the ECIs from one round of structural inversion, we use canonical Monte Carlo[49] (MC) simulation to do thermal annealing to find lower-energy configurations at each composition. Newly determined configurations are calculated within DFT and included in the next round of structural inversion and thermal annealing; the process continues until no new lower-energy GS configurations are found. For our initial structural inversion, we chose multiple structures at dilute Ag and Au compositions and around 50% Au. We also included some bulk-terminated structures from the Ag-Au bulk alloy GS, for example, finite clusters carved out of the bulk $L1_2$ at $Ag_{36}Au_{19}$ and $Ag_{19}Au_{36}$. For the MC-based thermal annealing, we start from 2784 K, decrease the temperature by a step size of 116 K until it reaches 116 K with 5000 equilibration MC steps at each temperature.

All DFT calculations were performed with PW91[50] exchange-correlation functional, utilizing a plane-wave basis set with the projected augmented wave method, as implemented in the Vienna Atomic Simulation Package (VASP).[51,52] The Γ-point with a Gaussian smearing of 0.1 eV and a kinetic energy cutoff of 400 eV were used to calculate total energies and relax structures. Total energies were converged below 2 meV/atom with respect to the sizes of k-point mesh and vacuum spacing. For ionic relaxation, the absolute magnitude of force on each atom was reduced below 0.02 eV/Å via conjugate gradient method.

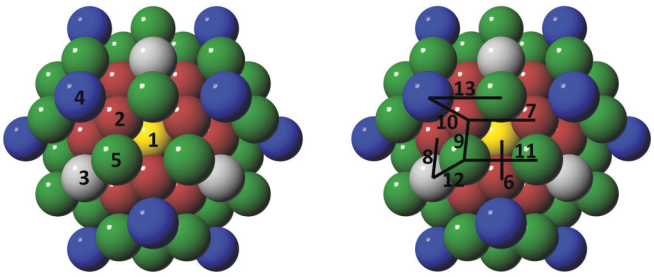

FIG. 1. (Color online) Distinctive (a) 1-body (single site) and (b) smallest 2-body (first pair) clusters in the CE for a 55-atom TC NP. The atomic sites are color-coded to show the five nonequivalent sites due to O_h symmetry as central-core (yellow), second-core (red), (100)-center (grey), corner (blue), and edge (green).

III. RESULTS AND DISCUSSION

In a 55-atom TC NP with fcc-stacking, the O_h symmetry reduces the number of nonequivalent atomic sites to five, shown in different colors in Fig. 1. There are 1 central-core, 12 second-core, 6 (100)-center, 12 corner, and 24 edge sites. As a result, the number of distinctive clusters in CE is greatly reduced. We show also in Fig. 1(a) the distinctive five 1-body (single site) and Fig. 1(b) the eight smallest 2-body (first pair) clusters, numbered consecutively as they appear in our CE. From a pool of 5 1-body, 45 2-body, 33 3-body, and 21 4-body clusters, an optimally truncated CE with the minimum leave-one-out cross-validation (CV-1) score is selected.

After three rounds of structural inversion in CE and thermal annealing with MC simulation, no new GS were found for the Ag-Au 55-atom TC NP. Figure 2 shows these results and the final GS hull. There are more GSs appearing at different compositions than the three GSs for Ag-Au bulk alloy. Seven GSs with their configurations are highlighted in Fig. 2 to show the specific site preferences. Starting at the dilute concentration of Au, for $Ag_{52}Au_3$, all three Au atoms occupy the edge sites on the shell with maximum separation. As Au content increases, for $Ag_{40}Au_{15}$, other edge and some corner sites on the shell become occupied. Interestingly the central-core site is also occupied by an Au atom. More importantly, this preference of Au atom for the central-core site persists at higher Au contents.

At $Ag_{36}Au_{19}$, the GS has a particular configuration with Au occupying the central-core site, all the corner sites and (100)-center sites on the shell, while Ag occupies all the second-core sites and edge sites on the shell. The configuration exhibits the bulk-terminated $L1_2$ Ag_3Au structure, but it is an off-stoichiometric phase and the only GS that resembles that of the bulk. Note usually Au does not prefer to occupy the (100)-center site on the shell. As the stoichiometry changes with increasing Au content to $Ag_{26}Au_{29}$, the central-core and second-core sites are fully occupied by Au and Ag, respectively. On the shell, Ag occupies all the (100)-center

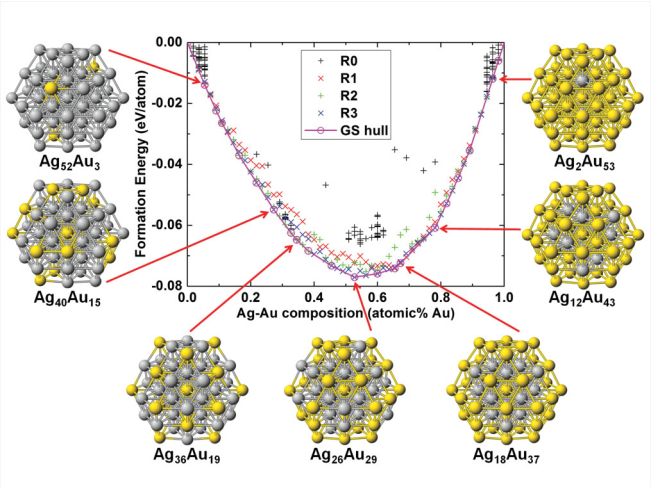

FIG. 2. (Color online) Ground state hull and atomic configurations for Ag-Au 55-atom TC NP. Grey (yellow) sphere stands for Ag (Au) atoms. DFT data determined the GS hull with three rounds (R1, R2, and R3) of CE structural inversion and thermal annealing. Seven GS with their atomic configurations are highlighted.

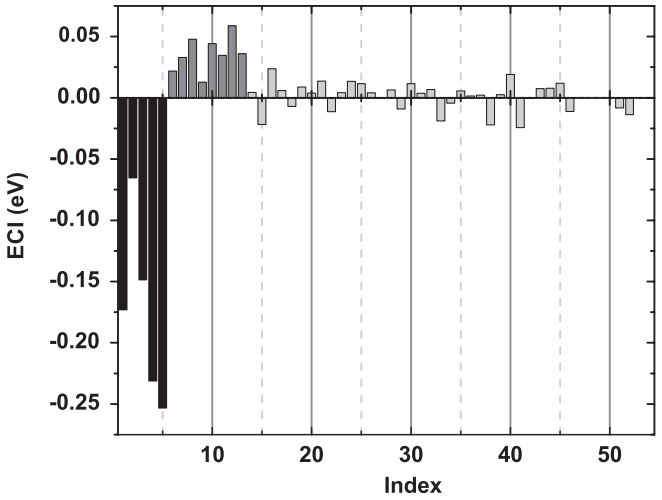

FIG. 3. ECIs of the optimal CE. Indices from 1 to 5 are 1-body (black) and from 6 to 13 (dark gray) are first-pair ECIs, followed by (light gray) higher 2-body (three 2nd, six 3rd, four 4th, five 5th, two 6th, four 7th, three 8th, three 9th, one 10th, and two 11th pairs) and two largest 3-body ECIs.

sites and other sites, while Au occupies the remaining corner and edge sites. Such multiple site preferences become clearer with more Au content at $Ag_{18}Au_{37}$, where Au occupies all the corner and edge sites on the shell as well as the central core site, leaving all the (100)-center sites on the shell and second-core sites to Ag (a configuration with the perfect O_h symmetry). The configuration is special in that it is a multishell or "onion-like" configuration with an embedded Ag shell inside the Au NP. For the GS at the nearby composition of $Ag_{19}Au_{36}$, an extra Ag atom occupies one of the edge sites in the perfect O_h GS of $Ag_{18}Au_{37}$. At this composition, there is also the bulk-terminated $L1_2$ structure with Ag occupying the central-core site whose DFT energy is 30 meV/atom above that of the GS found via thermal annealing.

Because of the overall preference for Au segregation to shell and Ag to core, one would wonder about the stability of perfect core-shell configuration at $Ag_{13}Au_{42}$. Our results show that there is no GS at this composition. At the nearby composition of $Ag_{12}Au_{43}$, most Ag atoms occupy the second-core sites, but there are still four Ag atoms at the (100)-center sites on the shell. This structure is 6 meV/atom lower than the perfect structure where all 12 Ag atoms are at the second-core sites. This reveals the delicate balance between the 1-body and higher-body ECIs in the NP. Finally, at Ag_2Au_{53}, the GS has two Ag atoms occupying the second-core sites—now farthest from each other.

We plot the ECI in Figure 3 for the optimal CE. The first five ECIs are 1-body and, as in the bulk alloy, they are all negative; the differences among the 1-body ECIs affect site preferences for Ag-Au. The next eight ECIs are the first pairs and are all positive, so Ag and Au favor unlike pairs, as in bulk. The averaged values of the 1-body and the smallest 2-body ECIs are close to their counterparts in bulk alloy. The magnitude of 1-body ECI is much larger than the first pairs, which is in turn much larger than the higher 2-body and 3-body ECIs. So the Ag-Au NP is still a nearest-neighbor pair dominated system.

The ECIs for 1-body and first pairs have large distributions. The specific site preference in the configurations on GS hull from DFT calculations is correlated with the magnitudes of these ECIs. Because Au is used as the solute, these different values elucidate the specific site preference when Au substitutes Ag, as ECIs correspond to the specific cluster configurations (see Fig. 1). As shown in Fig. 3, among the five 1-body ECIs, the fifth is the largest, while the second has the smallest absolute value. They correspond to edge and second-core sites, respectively. This means on substitution of Ag, Au prefers to first occupy the edge, then corner, central-core, and (100)-center sites, and last the second-core site, which agrees well with the trend found in the GS configurations in Fig. 2 with an increasing Au content. Thus, Ag favorably occupies the least preferred (second-core) site for Au. With the nearest-neighbor 2-body ECIs all positive, an energy

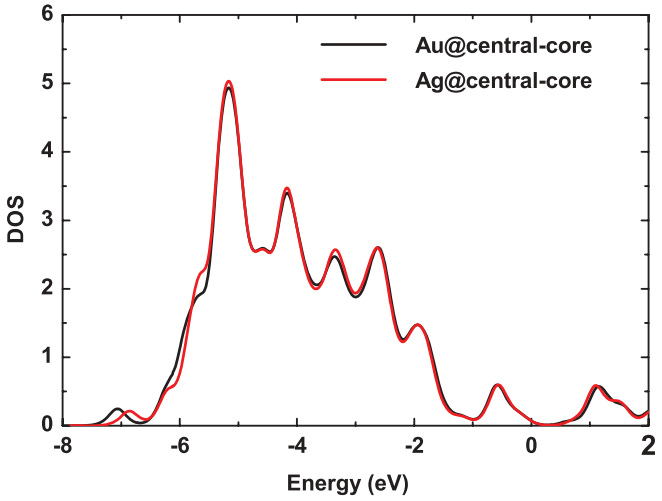

FIG. 4. (Color online) Projected density of states on one of the 12 Ag atoms occupying the second-core sites for $Ag_{18}Au_{37}$ ($Ag_{19}Au_{36}$) with Au (Ag) at the central-core site.

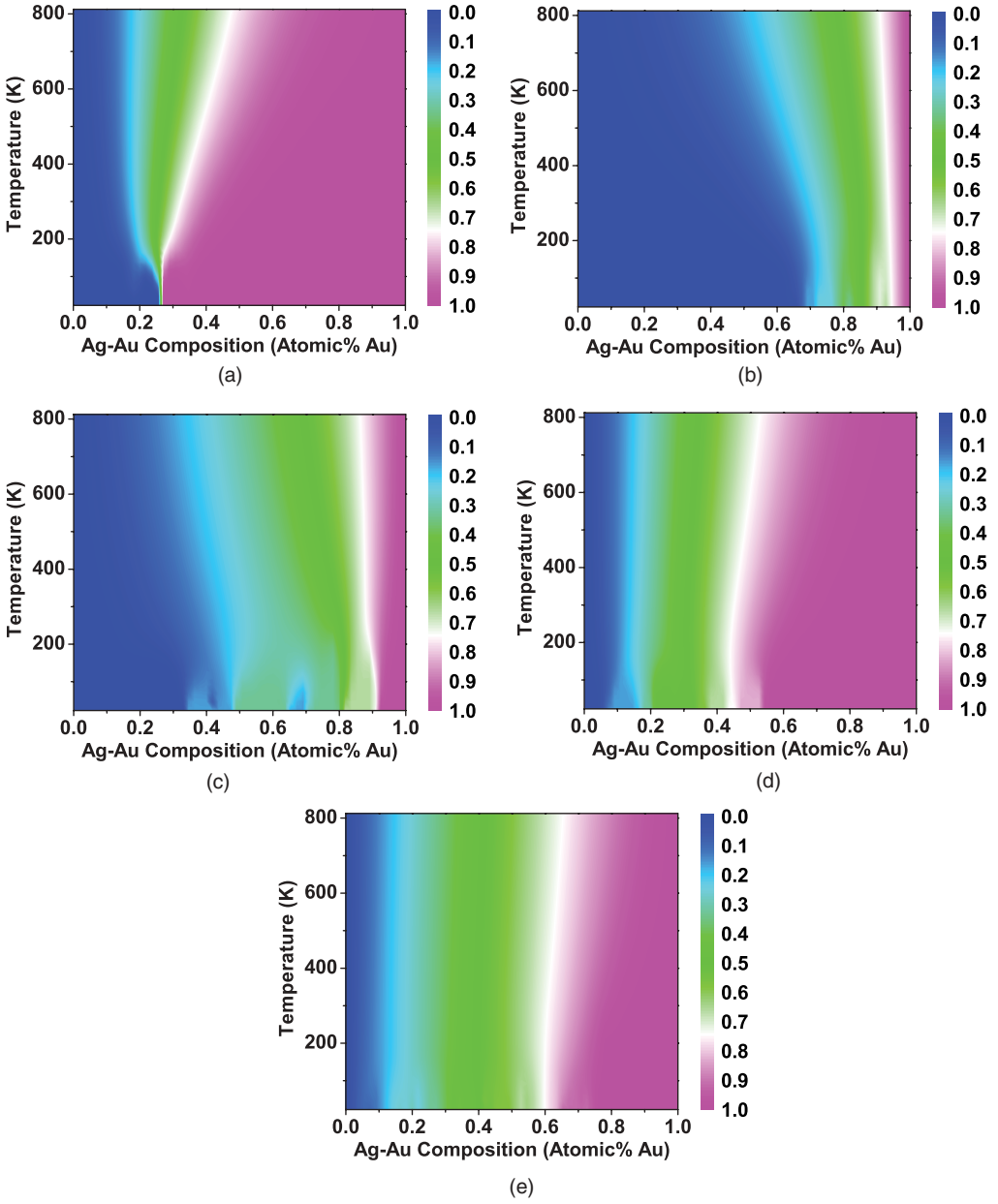

FIG. 5. (Color online) Site occupation (color map) as functions of c and T for the 55-atom Ag-Au TC NP for (a) central-core, (b) second-core, (c) (100)-center, (d) corner, and (e) edge sites.

cost is incurred for Au-Au occupation, so Ag-Au pairs are preferred. The largest first pair is the 12th ECI corresponding to the interaction between an edge and a (100)-center site on the shell. So, given the largest 1-body ECI placing Au at the edge sites, the 12th ECI gives the preference for Ag to occupy the (100)-center sites.

For all GSs with an Au concentration larger than $Ag_{40}Au_{15}$, the central-core site is always occupied by Au. To explain this from electronic structure, we choose the $Ag_{18}Au_{37}$ GS having the embedded Ag shell configuration with the perfect O_h symmetry. It is informative to see the difference in density of states (DOS) if the central-core site is replaced by Ag. Figure 4 shows the DOS projected on one of the 12 Ag atoms occupying the second-core sites with the central-core site being either Au or Ag. Clearly, when the central-core site is Au instead of Ag, there are more DOS on Ag appearing in lower energy, for a stronger binding to the Ag at these second-core sites. This agrees with the analysis using ECI that the unlike nearest pairs are favored. Because Au prefers most of the sites on the outer shell and Ag prefers the inner shell, to maximize the number of unlike nearest-neighbor pairs in a three-shell TC NP, it is energetically favorable for the central-core site to be occupied by Au, thus giving a multishell configuration.

With ECIs from the optimal CE, it is now possible to consider the configurational thermodynamics, i.e., site occupation as a function of both composition and temperature. Excluding the contribution from vibrations, phase diagrams in terms of composition and temperature for each nonequivalent atomic site in the 55-atom Ag-Au TC NP are shown in Fig. 5. The site occupation is color-mapped with respect to temperature and

the overall composition. Blue (red) corresponds to occupation predominantly by Ag (Au) and green corresponds to an occupation around 50% Au. It is very clear that the central-core site remains dominated by Au even at high temperature [see Fig. 5(a)]. The preference for Au is even higher than the corner site [Fig. 5(d)] and edge site [Fig. 5(e)] on the shell with respect to composition. Ag dominates the second-core site the most [Fig. 5(b)] followed by the (100)-center site [Fig. 5(c)]. Again, from the 1-body ECI, the central-core site is only the third preferred site for Au after the edge and corner sites on the shell, and the pair repulsion between central-core and second-core is also only moderate. But because the strongest site preference is for Ag to be on the second-core site, the central-core becomes the most favorable site for Au. This can be seen in the compensating profiles of the two sites in Figs. 5(a) and 5(b) as a function of temperature. This shows the strong correlations among these sites. In contrast, the site occupations on the three shell sites show a less variation as temperature changes.

The phase diagram for site occupation provides detailed information for design and/or prediction for NP catalysis. Often catalytic active site depends on local occupation features for a few nearby sites together[9,10] (often called the "ensemble" effect in catalysis[11]). This c-T phase diagram for site occupation reveals that at what composition range such catalytic active site(s) will form and how stable they are with respect to temperature. For example, an overall Au composition beyond 0.6 is needed to form Au pairs on all the neighboring corner and edge sites on the shell [Figs. 5(d) and 5(e)]. On the other hand, if Au atoms on the corner sites are mostly desired for catalysis, then the overall Au composition should be kept between 0.5 and 0.6. This insight can only be obtained by the type of configurational thermodynamics (i.e., correlated site occupations) presented in the current study.

IV. CONCLUSION

Using cluster expansion method coupled with DFT calculations, we have directly determined the composition-temperature phase diagram for a 55-atom Ag-Au truncated cuboctahedron nanoparticle and revealed the detailed site occupations as functions of both composition and temperature (configurational thermodynamics). Such information provides design information for alloyed nanoparticles, especially the thermodynamically stable active sites for catalysis. While generically Ag (Au) prefers the core (shell), agreeing with our universal core-shell preference behavior determined from the impurity segregation energy, the present approach gives specific site preferences for each stoichiometry and temperature, relevant to processing. With this information available, alloyed nanoparticles can be designed for specific active sites for catalysis with thermodynamic stability.

ACKNOWLEDGMENTS

Work at Ames Laboratory was supported by the US Department of Energy, Office of Basic Energy Sciences, Division of Materials Science and Engineering, with partial support for catalysis from the Division of Chemical Science, Geosciences, and Bioscience (DEFG02-03ER15476). Ames Laboratory is operated for DoE by Iowa State University under Contract No. DE-AC02-07CH11358. Initial support for T.L.T. to develop TTK was from National Science Foundation Grant DMR-012448 and the Materials Computation Center Grant DMR-0325939.

*llw@ameslab.gov
†ddj@ameslab.gov

[1] Ai-Qin Wang, Jun-Hong Liu, S. D. Lin, Tien-Sung Lin, and Chung-Yuan Mou, J. Catal. **233**, 186 (2005).
[2] Ai-Qin Wang, Chun-Ming Chang, and Chung-Yuan Mou, J. Phys. Chem. B **109**, 18860 (2005).
[3] Chun-Wan Yen, Meng-Liang Lin, Aiqin Wang, Shin-An Chen, Jin-Ming Chen, and Chung-Yuan Mou, J. Phys. Chem. C **113**, 17831 (2009).
[4] Nirmalya K. Chaki, Hironori Tsunoyama, Yuichi Negishi, Hidehiro Sakurai, and Tatsuya Tsukuda, J. Phys. Chem. C **111**, 4885 (2007).
[5] Hai-Long Jiang, Tomoki Akita, Tamao Ishida, Masatake Haruta, and Qiang Xu, J. Am. Chem. Soc. **133**, 1304 (2011).
[6] S. Link, C. Burda, Z. L. Wang, and M. A. El-Sayed, J. Chem. Phys. **111**, 1255 (1999).
[7] Huazhong Shi, Lide Zhang, and Weiping Cai, J. Appl. Phys. **87**, 1572 (2000).
[8] C. M. Chang, C. Cheng, and C. M. Wei, J. Chem. Phys. **128**, 124710 (2008).
[9] F. Besenbacher, I. Chorkendorff, B. S. Clausen, B. Hammer, A. M. Molenbroek, J. K. Nørskov, and I. Stensgaard, Science **279**, 1913 (1998).
[10] Georgios Kyriakou, Matthew B. Boucher, April D. Jewell, Emily A. Lewis, Timothy J. Lawton, Ashleigh E. Baber, Heather L. Tierney, Maria Flytzani-Stephanopoulos, and E. Charles H. Sykes, Science **335**, 1209 (2012).
[11] F. Maroun, F. Ozanam, O. M. Magnussen, and R. J. Behm, Science **293**, 1811 (2001).
[12] Michael S. Nashner, Anatoly I. Frenkel, David L. Adler, John R. Shapley, and Ralph G. Nuzzo, J. Am. Chem. Soc. **119**, 7760 (1997).
[13] Michael S. Nashner, Anatoly I. Frenkel, David Somerville, Charles W. Hills, John R. Shapley, and Ralph G. Nuzzo, J. Am. Chem. Soc. **120**, 8093 (1998).
[14] Sergio I. Sanchez, Matthew W. Small, Jian-min Zuo, and Ralph G. Nuzzo, J. Am. Chem. Soc. **131**, 8683 (2009).
[15] Matthew W. Small, Sergio I. Sanchez, Laurent D. Menard, Joo H. Kang, Anatoly I. Frenkel, and Ralph G. Nuzzo, J. Am. Chem. Soc. **133**, 3582 (2011).
[16] P. Hohenberg and W. Kohn, Phys. Rev. **136**, B864 (1964).
[17] W. Kohn and L. J. Sham, Phys. Rev. **140**, A1133 (1965).
[18] J. M. Sanchez, F. Ducastelle, and D. Gratias, Physica A: Stat. Mech. Appl. **128**, 334 (1984).
[19] J. M. Sanchez, J. P. Stark, and V. L. Moruzzi, Phys. Rev. B **44**, 5411 (1991).

[20]M. Asta, C. Wolverton, D. de Fontaine, and H. Dreyssé, Phys. Rev. B **44**, 4907 (1991).
[21]C. Wolverton, M. Asta, H. Dreyssé, and D. de Fontaine, Phys. Rev. B **44**, 4914 (1991).
[22]Marcel H. F. Sluiter, Y. Watanabe, D. de Fontaine, and Y. Kawazoe, Phys. Rev. B **53**, 6137 (1996).
[23]A. van de Walle and G. Ceder, J. Phase Equilib. **23**, 348 (2002).
[24]Nikolai A. Zarkevich and D. D. Johnson, Phys. Rev. Lett. **92**, 255702 (2004).
[25]Volker Blum, Gus L. W. Hart, Michael J. Walorski, and Alex Zunger, Phys. Rev. B **72**, 165113 (2005).
[26]Gus L. W. Hart, Volker Blum, Michael J. Walorski, and Alex Zunger, Nat. Mater. **4**, 391 (2005).
[27]N. A. Zarkevich, Teck L. Tan, and D. D. Johnson, Phys. Rev. B **75**, 104203 (2007).
[28]N. A. Zarkevich, Teck L. Tan, L. L. Wang, and D. D. Johnson, Phys. Rev. B **77**, 144208 (2008).
[29]Michael P. Mallin and Catherine J. Murphy, Nano Lett. **2**, 1235 (2002).
[30]Tomohiro Shibata, Bruce A. Bunker, Zhenyuan Zhang, Dan Meisel, Charles F. Vardeman, and J. Daniel Gezelter, J. Am. Chem. Soc. **124**, 11989 (2002).
[31]Chao Wang, Sheng Peng, Ryan Chan, and Shouheng Sun, Small **5**, 567 (2009).
[32]Matthew S. Shore, Junwei Wang, Aaron C. Johnston-Peck, Amy L. Oldenburg, and Joseph B. Tracy, Small **7**, 230 (2011).
[33]Madeeha A. Uppal, Michael B. Ewing, and Ivan P. Parkin, Euro. J. Inorganic Chem. **2011**, 4534 (2011).
[34]H. M. Chen, R. S. Liu, L. Y. Jang, J. F. Lee, and S. F. Hu, Chem. Phys. Lett. **421**, 118 (2006).
[35]Xiaoyan Liu, Aiqin Wang, Xiaofeng Yang, Tao Zhang, Chung-Yuan Mou, Dang-Sheng Su, and Jun Li, Chem. Mater. **21**, 410 (2008).
[36]D. Belic, R. L. Chantry, Z. Y. Li, and S. A. Brown, Appl. Phys. Lett. **99**, 171914 (2011).
[37]Fuyi Chen, Benjamin C. Curley, Giulia Rossi, and Roy L. Johnston, J. Phys. Chem. C **111**, 9157 (2007).
[38]Fuyi Chen and Roy L. Johnston, ACS Nano **2**, 165 (2007).
[39]Daojian Cheng, Wenchuan Wang, Shiping Huang, and Dapeng Cao, J. Phys. Chem. C **112**, 4855 (2008).
[40]F. Calvo, E. Cottancin, and M. Broyer, Phys. Rev. B **77**, 121406(R) (2008).
[41]L. Deng, W. Y. Hu, H. Q. Deng, S. F. Xiao, and J. F. Tang, J. Phys. Chem. C **115**, 11355 (2011).
[42]Fuyi Chen and Roy L. Johnston, Acta Mater. **56**, 2374 (2008).
[43]Lauro Oliver Paz-Borbon, Roy L. Johnston, Giovanni Barcaro, and Alessandro Fortunelli, J. Chem. Phys. **128**, 134517 (2008).
[44]Hannu Häkkinen and Uzi Landman, Phys. Rev. B **62**, R2287 (2000).
[45]M. Cerbelaud, R. Ferrando, G. Barcaro, and A. Fortunelli, PhysChemChemPhys **13**, 10232 (2011).
[46]Lin-Lin Wang and Duane D. Johnson, J. Am. Chem. Soc. **131**, 14023 (2009).
[47]J. W. D. Connolly and A. R. Williams, Phys. Rev. B **27**, 5169 (1983).
[48]I. A. Abrikosov, A. V. Ruban, H. L. Skriver, and B. Johansson, Phys. Rev. B **50**, 2039 (1994).
[49]N. Metropolis, A. W. Rosenbluth, M. N. Rosenbluth, A. H. Teller, and E. Teller, J. Chem. Phys. **21**, 1087 (1953).
[50]J. P. Perdew and Y. Wang, Phys. Rev. B **45**, 13244 (1992).
[51]G. Kresse and J. Furthmuller, Phys. Rev. B **54**, 11169 (1996).
[52]G. Kresse and J. Furthmuller, Comput. Mater. Sci. **6**, 15 (1996).